Scientia Iranica B (2013) 20(5), 1474–1484

Sharif University of Technology
Scientia Iranica
Transactions B: Mechanical Engineering
www.scientiairanica.com

Heat and mass transfer by natural convection around a hot body in a rectangular cavity

G.A. Sheikhzadeh[a], R. Heydari[a], N. Hajialigol[a,*], A. Fattahi[a] and M.A. Mehrabian[b]

a. *Department of Mechanical Engineering, University of Kashan, Kashan, P.O. Box 87317-51167, Iran.*
b. *Department of Mechanical Engineering, Shahid Bahonar University of Kerman, Iran.*

Received 1 February 2012; received in revised form 7 December 2012; accepted 6 May 2013

KEYWORDS
Heat and mass transfer;
Natural convection;
Cavity.

Abstract. The simultaneous heat and mass transfer by natural convection around a hot body in a rectangular cavity is investigated numerically. The cavity is filled with air and the ratio of body's length to enclosure's length is assumed to be constant at 1/3. The differential equations for continuity, momentum, energy and mass transfer are solved using the Patankar technique. The results are displayed in the form of isotherms, isoconcentrations and streamlines, and the effects of Rayleigh number, Lewis number and buoyancy ratio on average Sherwood and Nusselt numbers are investigated. The study covers a wide range of Rayleigh numbers, Lewis numbers, and buoyancy ratios. It is observed that by increasing Lewis number, the average Sherwood number increases and the average Nusselt number decreases. Additionally, by increasing the absolute value of buoyancy ratio, the average Sherwood and Nusselt numbers enhance. This work presents a novel approach in this field in the light of geometry and the range of dimensionless numbers.

1. Introduction

Natural convection has become the subject of many experimental and numerical studies in recent years due to its widespread applications in engineering and industry, such as cooling of electronic systems, float glass manufacturing, solar ponds and metal solidification processes. Davis [1] investigated a benchmark for numerical solution on natural convection of air in a square enclosure. Ostrach [2] traced out the rich diversity of natural convection problems in science and technology. The numerous studies have focused extensively on convective flows driven by the density inversion effect [3-10].

The steady-state flow structure, temperature and heat transfer in a square enclosure, heated and cooled on opposite vertical walls and containing cold water, are numerically investigated by Lin and Nansteel [3]. Nansteel et al. [4] studied the natural convection of water in the vicinity of its maximum density in a rectangular enclosure in the limit of small Rayleigh number. They observed that the strength of the counter rotating flow decreases with decreasing aspect ratio. Hossain and Rees [8] studied the natural convection in an enclosure with heat generation. In this analysis, when the heat generation parameter is sufficiently strong, the circulation of the flow is reversed.

Lee and Ha [11] numerically investigated natural convection in a horizontal enclosure with a conducting body. They compared the results of the case of conducting body with those of adiabatic and neutral isothermal bodies. They showed that when the dimensionless thermal conductivity is 0.1, a pattern of fluid

*. *Corresponding author.*
E-mail address: Najmeh.Hajialigol@gmail.com (N. Hajialigol)

flow and isotherms and the corresponding surface- and time-averaged Nusselt numbers are almost the same as the case of an adiabatic body.

Das and Reddy [12] studied natural convection flow in a square enclosure with a centered internal conducting square block both having an inclination angle using SIMPLE algorithm. They considered an angle of inclination in the range of 15-90 degrees and ratio of solid to fluid thermal conductivities of 0.2 and 5. Sheikhzadeh et al. [13,14] studied the steady magneto-convection around an adiabatic body inside a square enclosure.

The simultaneous heat and mass transfer occurs in many processes in industry and engineering equipment and environmental applications, involving the transport of water vapor and other chemical contaminants across enclosed spaces. Comparison of the scales of the two buoyancy terms in the momentum equation suggests three classes of flows:

(i) Heat transfer driven flows when the buoyancy effect, due to heating from the sides, is dominant;

(ii) Combined heat and mass transfer driven flows when both buoyancy terms are important;

(iii) Mass transfer driven flows, when the buoyancy, due to heating from the sides, is negligible.

The distinction between these flows can be made using the buoyancy ratio (N); $|N|\langle O(1)$ for class (i), $|N| \sim O(1)$ for class, (ii), and $|N|\rangle O(1)$ for class (iii).

Gebhart and Pera [15], using the similarity method, investigated the laminar flows which arise in fluids due to the interaction of the force of gravity and density differences caused by the simultaneous diffusion of thermal energy and chemical species. Bejan [16] presented a fundamental study of laminar natural convection in a rectangular enclosure with heat and mass transfer from the side. He used scale analysis to determine the scales of the flow, temperature and concentration fields in boundary layer flow for all values of Prandtl and Lewis numbers. He investigated the case of $N = 0$ to study the heat-transfer-driven flows. Wee et al. [17] investigated numerically and experimentally the same problem for both horizontal and vertical cavity. The experimental technique employed two porous plastic plates as two cavity walls allowing the imposition of simultaneous moisture and temperature gradients.

Nishimura et al. [18] studied numerically the oscillatory double-diffusive convection in a rectangular enclosure with combined horizontal temperature and concentration gradients. Natural convection flow, resulting from the combined buoyancy effects of thermal and mass diffusion in a cavity with differentially heated sidewalls, was numerically studied by Snoussi et al. [19]. They considered a wide range of Rayleigh numbers and used finite-element method. They showed that mass and temperature fields are strongly dependent on thermal Rayleigh number and the aspect ratio of the cavity. Chouikh et al. [20] studied numerically the natural convection flow resulting from the combined buoyancy effects of thermal and mass diffusion in an inclined glazing cavity with differentially heated side walls. The double-diffusive natural convection of water in a partially heated enclosure with Soret and Dufour effects is numerically studied by Nithyadevi and Yang [21]. The effect of various parameters such as thermal Rayleigh number, buoyancy ratio number, Schmidt number and Soret and Dufour coefficients on the flow pattern, heat and mass transfer was depicted. Nikbakhti and Rahimi [22] studied double-diffusive natural convection in a rectangular cavity with partially thermal active side walls. They found that in aiding flow, heat transfer increases by increasing the buoyancy ratio. Their results also showed that in opposing flow, with increasing buoyancy ratio until unity, heat transfer decreases.

Al-Amiri et al. [23] and Teamah and Maghlany [24] studied the heat and mass transfer in a lid-driven cavity. More recently, Mahapatra et al. [25] analyzed the effects of uniform and non-uniform heating of wall(s) on double-diffusive natural convection in a lid-driven square enclosure.

In the present study, natural convection around a hot body in a square cavity filled with air is studied numerically, using the finite volume method. Simultaneous heat and mass transfer and the effects of pertinent parameters such as buoyancy ratio, Rayleigh and Lewis numbers on the flow are studied. Despite numerous works in this field, to the best of authors' knowledge, no similar study has been carried out to simulate simultaneous heat and mass transfer in the current geometry with the range of buoyancy ratio, Rayleigh and Lewis numbers used in this study.

2. Mathematical model

A schematic diagram of the enclosure with coordinate system and boundary conditions is shown in Figure 1. Both body and enclosure walls are held at constant but different temperatures and concentrations; high temperature and concentration (T_h, C_h) for the body and low temperature and concentration (T_c, C_c) for the cavity are considered. In this study, the ratio of W/L is maintained constant at 1/3, and the body is located in the center of the cavity.

The Boussinesq approximation holds, meaning that density is linearly proportional to both temperature and concentration.

$$\rho = \rho_0 \left(1 - \beta_T(T - T_c) - \beta_M(c - c_c)\right). \qquad (1)$$

With these assumptions, two dimensional laminar

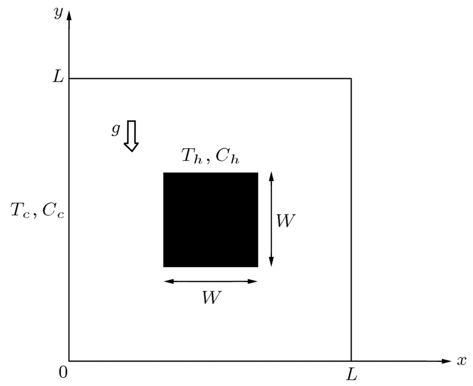

Figure 1. Geometry and boundary conditions.

governing equations including continuity, momentum, concentration and energy in steady state conditions can be written as:

Continuity equation:

$$\frac{\partial u}{\partial x}+\frac{\partial v}{\partial y}=0. \tag{2}$$

x-momentum equation:

$$u\frac{\partial u}{\partial x}+v\frac{\partial u}{\partial y}=-\frac{1}{\rho}\frac{\partial p}{\partial x}+\upsilon\left(\frac{\partial^2 u}{\partial x^2}+\frac{\partial^2 u}{\partial y^2}\right). \tag{3}$$

y-momentum equation:

$$u\frac{\partial v}{\partial x}+v\frac{\partial v}{\partial y}=-\frac{1}{\rho}\frac{\partial p}{\partial y}+\upsilon\left(\frac{\partial^2 v}{\partial x^2}+\frac{\partial^2 v}{\partial y^2}\right)$$
$$+g[\beta_T(T-T_c)+\beta_M(c-c_c)]. \tag{4}$$

Energy equation:

$$u\frac{\partial T}{\partial x}+v\frac{\partial T}{\partial y}=\alpha\left(\frac{\partial^2 T}{\partial x^2}+\frac{\partial^2 T}{\partial y^2}\right). \tag{5}$$

Concentration equation:

$$u\frac{\partial c}{\partial x}+v\frac{\partial c}{\partial y}=D\left(\frac{\partial^2 c}{\partial x^2}+\frac{\partial^2 c}{\partial y^2}\right). \tag{6}$$

Using the dimensionless variables:

$$X=\frac{x}{L},\qquad Y=\frac{y}{L},\qquad U=\frac{uL}{\alpha},$$
$$V=\frac{vL}{\alpha},\qquad P=\frac{p}{\rho}\frac{L^2}{\alpha^2},\qquad \theta=\frac{T-T_c}{T_h-T_c},$$
$$C=\frac{c-c_c}{c_h-c_c}, \tag{7}$$

the dimensionless form of the equations become:

$$\frac{\partial U}{\partial X}+\frac{\partial V}{\partial Y}=0, \tag{8}$$

$$U\frac{\partial U}{\partial X}+V\frac{\partial U}{\partial Y}=-\frac{\partial P}{\partial X}+\Pr\left(\frac{\partial^2 U}{\partial X^2}+\frac{\partial^2 U}{\partial Y^2}\right), \tag{9}$$

$$U\frac{\partial V}{\partial X}+V\frac{\partial V}{\partial Y}=-\frac{\partial P}{\partial Y}+\Pr\left(\frac{\partial^2 V}{\partial X^2}+\frac{\partial^2 V}{\partial Y^2}\right)$$
$$+\mathrm{Ra}_T\Pr(\theta+NC), \tag{10}$$

$$U\frac{\partial \theta}{\partial X}+V\frac{\partial \theta}{\partial Y}=\frac{\partial^2 \theta}{\partial X^2}+\frac{\partial^2 \theta}{\partial Y^2}, \tag{11}$$

$$U\frac{\partial C}{\partial X}+V\frac{\partial C}{\partial Y}=\frac{1}{\mathrm{Le}}\left(\frac{\partial^2 C}{\partial X^2}+\frac{\partial^2 C}{\partial Y^2}\right). \tag{12}$$

The thermal and mass Rayleigh numbers, Lewis number, Prandtl number, and buoyancy ratio in the above equations are defined as:

$$\mathrm{Ra}_T=\frac{g\beta_T L^3\Delta T}{\alpha\upsilon},$$
$$\mathrm{Ra}_M=\frac{g\beta_M L^3\Delta c}{D\upsilon}=\mathrm{Ra}_T\mathrm{Le}N,$$
$$\mathrm{Le}=\frac{\alpha}{D},$$
$$\Pr=\frac{\upsilon}{\alpha},$$
$$N=\frac{\beta_M\Delta c}{\beta_T\Delta T}, \tag{13}$$

where β_T and β_M are thermal and concentration expansion coefficients. β_T is positive but β_M can be negative or positive [16]:

$$\beta_T=-\frac{1}{\rho}\left(\frac{\partial\rho}{\partial T}\right)_P,$$
$$\beta_M=-\frac{1}{\rho}\left(\frac{\partial\rho}{\partial c}\right)_P. \tag{14}$$

The values of β_M for some species are presented by Gebhart and Pera [15].

Dimensionless boundary conditions are as follows:

$0\le X\le 1\rightarrow$

$$U(X,0)=U(X,1)=V(X,0)=V(X,1)=0,$$
$$\theta(X,0)=\theta(X,1)=C(X,0)=C(X,1)=0.$$

$0\le Y\le 1\rightarrow$

$$U(0,Y)=U(1,Y)=V(0,Y)=V(1,Y)=0,$$
$$\theta(0,Y)=\theta(1,Y)=C(0,Y)=C(1,Y)=0.$$

$$\frac{L}{2}-\frac{W}{2}\leq X\leq \frac{L}{2}+\frac{W}{2}\rightarrow$$

$$U\left(X,\frac{L}{2}-\frac{W}{2}\right)=U\left(X,\frac{L}{2}+\frac{W}{2}\right)$$

$$=V\left(X,\frac{L}{2}-\frac{W}{2}\right)=V\left(X,\frac{L}{2}+\frac{W}{2}\right)=0,$$

$$\theta\left(X,\frac{L}{2}-\frac{W}{2}\right)=\theta\left(X,\frac{L}{2}+\frac{W}{2}\right)$$

$$=C\left(X,\frac{L}{2}-\frac{W}{2}\right)=C\left(X,\frac{L}{2}+\frac{W}{2}\right)=1.$$

$$\frac{L}{2}-\frac{W}{2}\leq Y\leq \frac{L}{2}+\frac{W}{2}\rightarrow$$

$$U\left(\frac{L}{2}-\frac{W}{2},Y\right)=U\left(\frac{L}{2}+\frac{W}{2},Y\right)$$

$$=V\left(\frac{L}{2}-\frac{W}{2},Y\right)=V\left(\frac{L}{2}+\frac{W}{2},Y\right)=0,$$

$$\theta\left(\frac{L}{2}-\frac{W}{2},Y\right)=\theta\left(\frac{L}{2}+\frac{W}{2},Y\right)$$

$$=C\left(\frac{L}{2}-\frac{W}{2},Y\right)=C\left(\frac{L}{2}+\frac{W}{2},Y\right)=1. \tag{15}$$

Local and average Nusselt and Sherwood numbers on the vertical left side hot wall are defined as follows:

$$\mathrm{Nu}=-\left(\frac{\partial\theta}{\partial X}\right)\Big|_{X=\frac{L}{2}-\frac{W}{2}}, \tag{16}$$

$$\mathrm{Nu}_a=-\frac{1}{A}\int_0^A\left(\frac{\partial\theta}{\partial X}\right)_{X=\frac{L}{2}-\frac{W}{2}}dY, \tag{17}$$

$$Sh=-\left(\frac{\partial C}{\partial X}\right)\Big|_{X=\frac{L}{2}-\frac{W}{2}}, \tag{18}$$

$$Sh_a=-\frac{1}{A}\int_0^A\left(\frac{\partial C}{\partial X}\right)_{X=\frac{L}{2}-\frac{W}{2}}dY. \tag{19}$$

In general, Sherwood number represents the mass transfer strength like Nusselt number that symbolizes the heat transfer strength.

3. Numerical method

The governing non-linear equations with appropriate boundary conditions were solved by iterative numerical method, using finite volume technique. In order to couple the velocity field and pressure in momentum equations, the well-known SIMPLER (Semi-Implicit Method for Pressure-Linked Equations Revised) algorithm was adopted. Uniform grid is used for this problem and grid independency test was performed. The discretized equations were solved by the Gausse-Seidel method. The iteration method used in this program is a line-by-line procedure which is a combination of the direct method and the resulting Three Diagonal Matrix Algorithm (TDMA). The diffusion terms in the equations are discretized by a second order central difference scheme, while a hybrid scheme (a combination of the central difference scheme and the upwind scheme) is employed to approximate the convection terms. The under-relaxation factors for U-velocity, V-velocity, energy and concentration equations were 0.6, 0.6, 0.4 and 0.4, respectively. The solution is terminated until the following convergence criterion is met:

$$\mathrm{Error}=\frac{\sum_{j=1}^{m}\sum_{i=1}^{n}\left|\xi^{t+1}-\xi^{t}\right|}{\sum_{j=1}^{m}\sum_{i=1}^{n}\left|\xi^{t+1}\right|}\leq 10^{-10}, \tag{20}$$

where m and n are the number of cells in X and Y directions, respectively, ξ is a transport quantity, and t is the number of iteration.

3.1. Code validation

To reach the grid independent solution, various grids (21×21, 61×61, 81×81 and 101×101) were tested for calculating the average Nusselt number on the hot walls (Table 1). The grid size of 81×81 is adequately appropriate to ensure a grid-independent solution.

Figures 2 and 3 present a comparison between the present work and the results of Lee and Ha [11] and

Table 1. Grid independency test for $\mathrm{Ra}_T=10^4$, $N=1$ and $\mathrm{Le}=1$.

Grid	21×21	61×61	81×81	101×101
$\mathbf{Nu}_a$	5.310	6.056	6.162	6.167

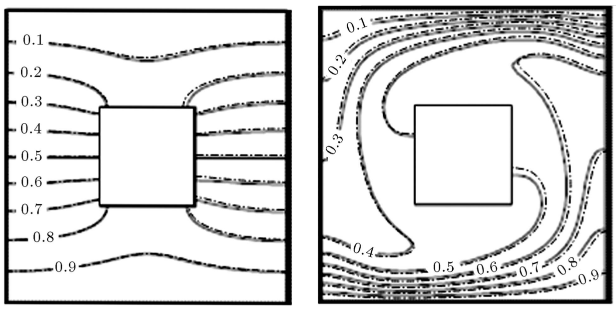

Figure 2. The comparison between Isotherms for adiabatic body at $\mathrm{Ra}=10^3$ (left) and $\mathrm{Ra}=10^4$ (right); Lee and Ha [11] (solid lines), present work (dashed line).

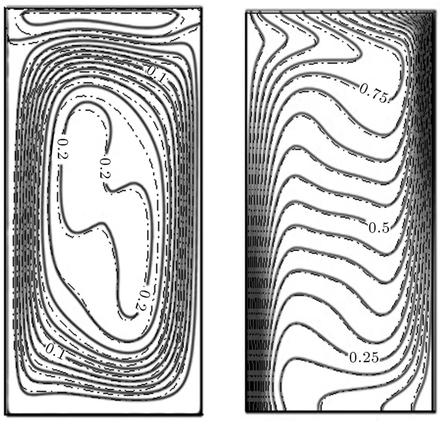

Figure 3. Isotherm (right), and stream line (left) for Le = 1, $N = 10$, Ri = 1 and $U_{\mathrm{up}} = -1$; Teamah [24] (solid lines), present work (dashed lines).

Teamah and Maghlany [24], respectively. It is obvious that the two sets of results are in good agreement.

4. Results and discussion

The present study considers the effects of buoyancy ratio ($-10 \leq N \leq 10$), Rayleigh number ($10^3 \leq \mathrm{Ra}_T \leq 10^5$) and Lewis number ($0.1 \leq \mathrm{Le} \leq 50$) on the isotherms, isoconcentrations, streamlines, average Nusselt number and average Sherwood number.

4.1. Effect of buoyancy ratio

Dependence of streamlines, isoconcentrations and isotherms on buoyancy ratio is shown in Figures 4, 5, and 6. Figure 7 shows the effect of N and Le number on average Sherwood and Nusselt numbers. To investigate the effect of buoyancy ratio, the thermal Rayleigh number is kept constant at 10^4, and Lewis numbers are chosen 0.1, 1 and 10. At all Lewis numbers and buoyancy ratios, two primary vortices are formed at the right and left sides of the hot body, respectively. By increasing the absolute value of N and Le number, the maximum absolute values of stream function for these primary vortices increase and decrease, respectively. Discussion about the effect of N on fluid flow, heat and mass transfer is done in three cases: $N > 0$, $N < 0$ and $N = 0$.

$N > 0$: At Le=1 and 10, by increasing the value of N from 0 to 10, two secondary vortices are appeared at the top of the hot body; the strength of these secondary vortices are lower than that of the primary vortices. At Le = 0.1, the mass diffusivity is higher than the thermal diffusivity and for all N, isoconcentration lines are approximately parallel to the walls (Figure 4). As shown in Figure 4, by increasing the buoyancy ratio, isotherms become denser near the bottom wall of the hot body, and two weak isothermal plumes are appeared at the top corners of the body. According to Figure 7, it is observed that by increasing the buoyancy ratio, the average Nusselt number increases but the average Sherwood number is approximately constant. Figure 7 shows also that the values of average Nusselt number for Le=0.1 are higher than those of Sherwood number. At Le=1, plots of isoconcentrations and isotherms are the same, and the average Nusselt number and Sherwood number are equal [11] and they increase with increasing N. According to Figure 5, two isothermal and isoconcentration plumes are appeared

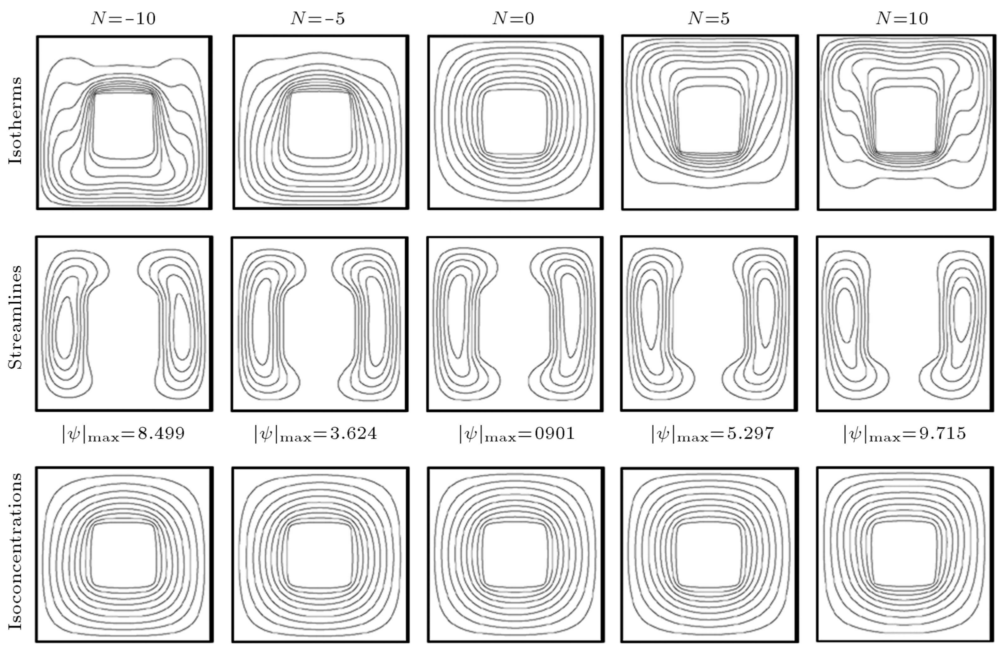

Figure 4. Isotherms, streamlines and isoconcentrations for Ra = 10^4 and Le = 0.1.

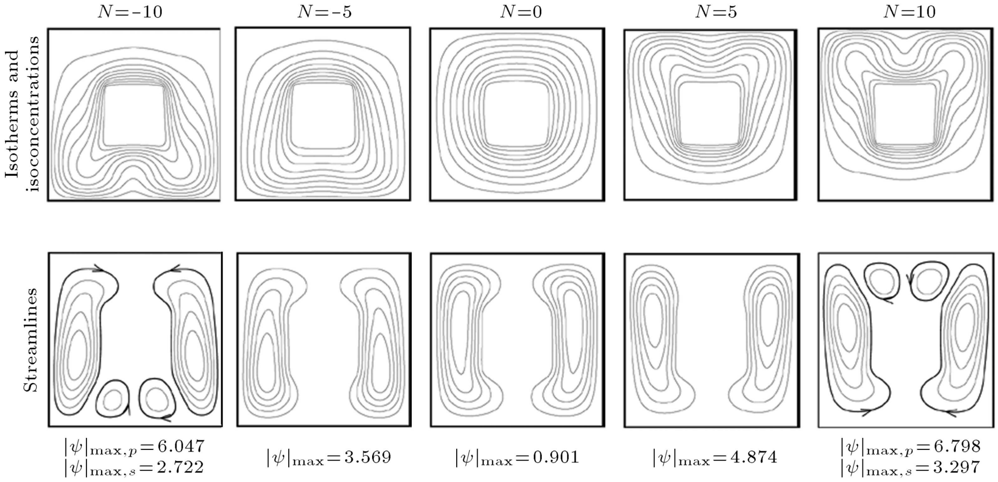

Figure 5. Isotherms, isoconcentrations and streamlines for $\mathrm{Ra} = 10^4$ and $\mathrm{Le} = 1$.

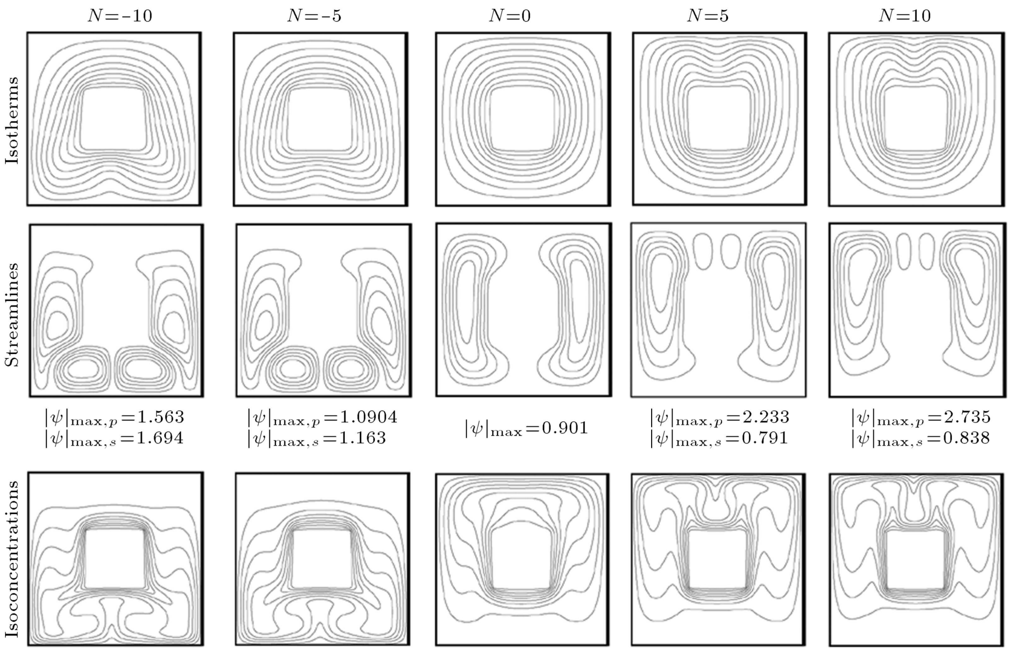

Figure 6. Isotherms, streamlines and isoconcentrations for $\mathrm{Ra} = 10^4$ and $\mathrm{Le} = 10$.

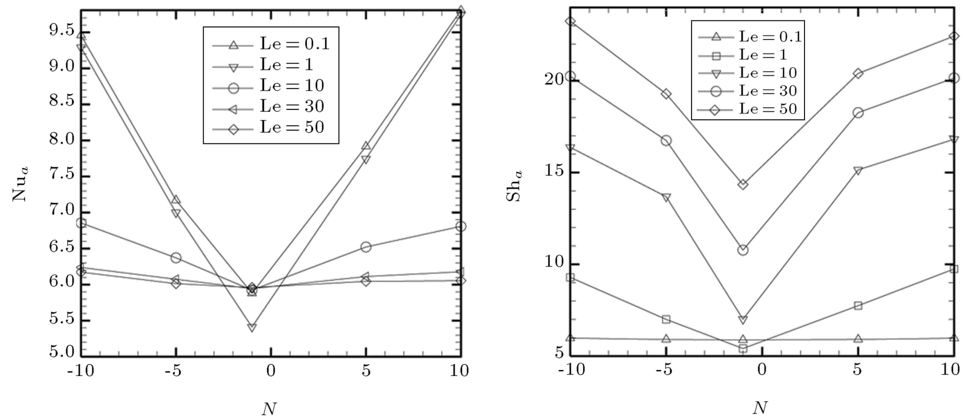

Figure 7. Effect of Lewis number and buoyancy ratio on average Sherwood and Nusselt numbers.

at the top corners of the body. At Le=10, the isoconcentration plumes are more obvious than the isothermal plumes.

$N < 0$: At Le=1 and 10, by decreasing N from 0 to -10, two secondary vortices are appeared at the bottom of the hot body. At Le=10, the strength of the secondary vortices bocomes more than that of the primary vortices. At Le=0.1, two weak isothermal plumes are appeared at the bottom corners of the hot body. It is also observed from Figure 7 that by decreasing N from -1 to -10, the average Nusselt number increases, but the average Sherwood number is approximately constant. At Le=1, two isothermal and isoconcentration plumes are appeared at the bottom corners of the hot body at $N = -10$ (Figure 5). By decreasing N from -1 to -10, the average Sherwood and Nusselt number increase (Figure 7). By decreasing N, both heat and mass transfer are increased. At Le=10, the formed isoconcentration plumes, at the bottom corners of the hot body, are more obvious than the isothermal plumes. At $N = -1$ and Le=1 there is no convection flow, and therefore the average Nusselt number and Sherwood number have their minimum values at this condition. As Figure 7 shows, at low Le, Sh_a and Nu_a are not a function of N.

$N = 0$: At $N = 0$, convection flow is formed only due to temperature gradient. One isoconcentration plume at the top of the hot body is appeared at Le=10.

Flow direction in the vortices for negative and positive values of N are shown in Figure 5; for instance at $N = 10$ (aiding effect of temperature and concentration gradients) and $N = -10$ (opposing effect of temperature and concentration gradients). It is observed that at $N = -10$, the primary vortex is CCW and the secondary vortex is CW at the right side of the hot body (in the direction caused by the predominant mass gradient), and at $N = 10$, the primary vortex is CW and the secondary vortex is CCW at the right side of the hot body.

4.2. Effect of Lewis number

The effect of Lewis number at Ra $= 10^4$ on plots of isotherms, isoconcentrations and streamlines for $N = 1$, 10 and -1 are shown in Figures 8, 9 and 10, respectively. When Le=1, the isotherms and isoconcentrations are similar to each other due to the similarity between the energy and concentration equations. It is observed that by increasing Le, convection flow suppresses and so the maximum absolute value of stream function decreases. At $N = 1$ for Le > 10 there is an isoconcentration plume at the top of the hot body. At $N = 10$, two secondary vortices and two plumes are appeared at the top of the hot body at Le=1 and 10. The secondary vortices vanish at Le=30 and 50, and two plumes become one plume. It is observed from Figure 9 that isoconcentration plumes are more obvious than that of isothermal plume. It is found from Figure 7 that mass transfer increases when Le

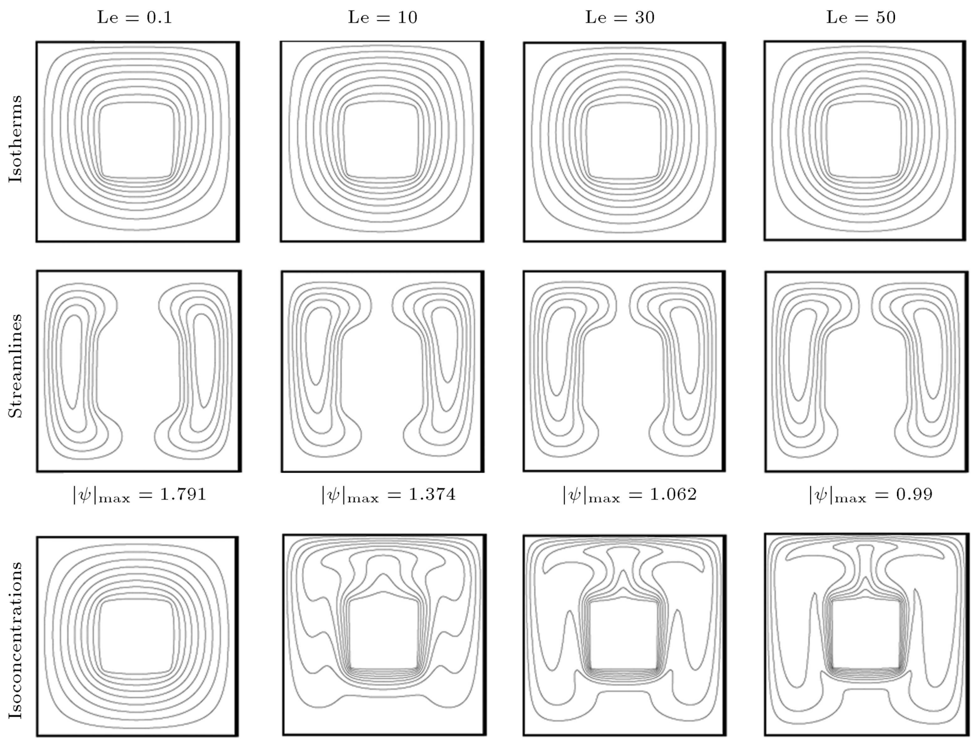

Figure 8. Isotherms, Isoconcenterations and streamlines for $N = 1$ and Ra $= 10^4$.

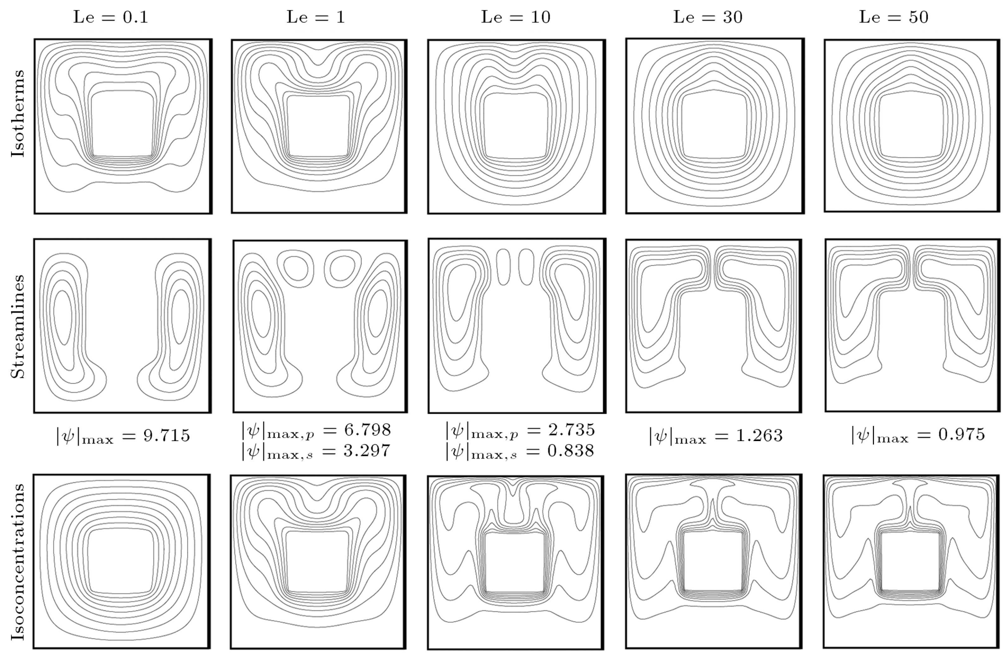

Figure 9. Isotherms, isoconcenterations and streamlines for $N = 10$ and $\mathrm{Ra} = 10^4$.

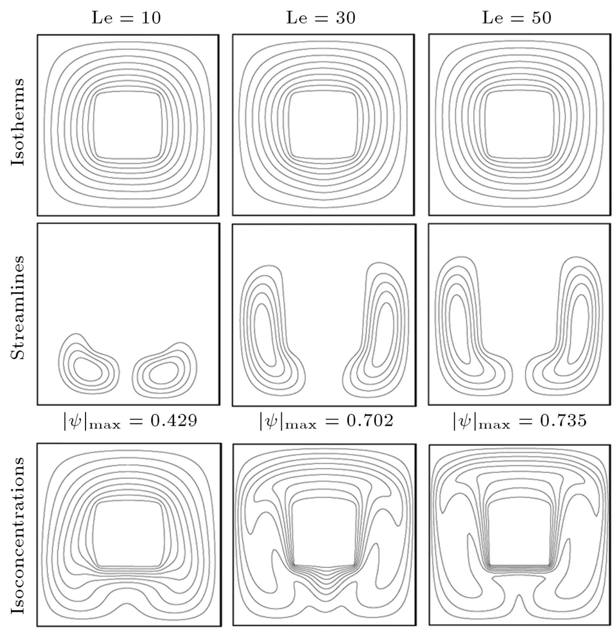

Figure 10. Isotherms, isoconcenterations and streamlines for $N = -1$ and $\mathrm{Ra} = 10^4$.

enhances as a result of densing solutal boundary layer (it is seen in Figure 8). On the other hand, Nu_a reduces when Le increases. As Le increases, thermal diffusivity increases ($\alpha = k/\rho c_p$). It causes conduction heat transfer to be stronger at high Le compared to the low Le cases where convection is stronger and dominant. Because conduction has a minor effect on heat transfer in comparison with convection, Nu decreases as Le increases.

The effect of Le on isotherms, isoconcentrations and streamlines at $N = -1$ is shown in Figure 10. The isotherms are approximately the same. It is observed that by increasing Le, the maximum absolute value of stream function increases.

Table 2. Correlations of Sh_a and Nu_a in terms of Le and N.

Range of N	**Correlation**
$N \succ 0$	$\mathrm{Sh}_a = 7.3167\mathrm{Le}^{0.2236} N^{0.1103}$
	$\mathrm{Nu}_a = 7.0775\mathrm{Le}^{-0.0764} N^{0.0818}$
$N \leq -1$	$\mathrm{Sh}_a = 5.2186\mathrm{Le}^{0.2379} \lvert N\rvert^{0.2418}$
	$\mathrm{Nu}_a = 6.4143\mathrm{Le}^{-0.0525} \lvert N\rvert^{0.0937}$

The predicted values of Sh_a and Nu_a in the ranges investigated for N and Le and at $\mathrm{Ra} = 10^4$ are correlated and presented in Table 2. The validity ranges for these correlations are $0.1 \leq \mathrm{Le} \leq 50$ and $-10 \leq N \leq 10$.

4.3. Effect of Rayleigh number

Effect of Rayleigh number on plots of isotherms, isoconcentrations and streamlines, for instance at $N = 1$ and Le=1, are shown in Figure 11. It is observed, as expected, that convection flow becomes stronger by increasing Ra, and the secondary vortices are appeared at $\mathrm{Ra} = 10^5$. Variations of Sh_a and Nu_a with respect to N at various Ra are shown in Figure 12. In this figure it is shown that Nu and Sh increase with Rayleigh number.

The predicted values of Sh_a and Nu_a over the ranges investigated for N and Ra and at Le=1 are correlated and presented in Table 3. The validity ranges for these correlations are: $0.1 \leq \mathrm{Le} \leq 50$ and

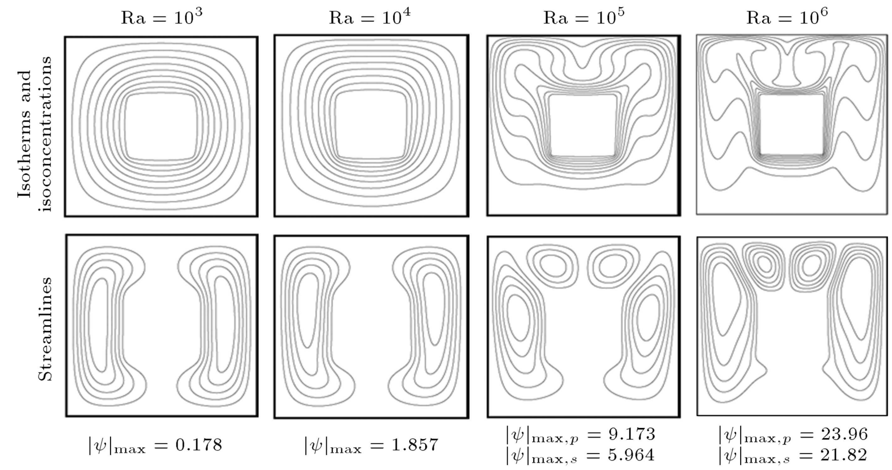

Figure 11. Effect of Rayleigh number on isotherms (and also isoconcentrations) and streamlines, for Le = 1 and $N = 1$.

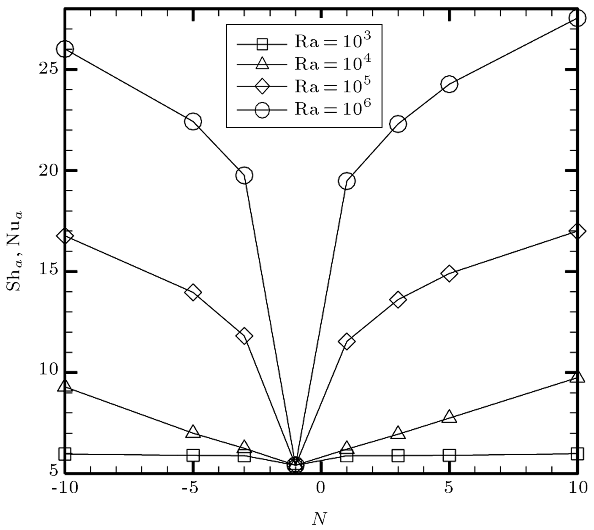

Figure 12. Effect of Rayleigh number on average Nusselt and Sherwood numbers on hot wall at Le = 1 and various N.

Table 3. Correlations of Sh_a and Nu_a in terms of Ra and N.

Range of N	**Correlation**
$N \succ 0$	$\mathrm{Nu}_a = \mathrm{Sh}_a = 0.91526\mathrm{Ra}^{0.2198}N^{0.1557}$
$N \leq -1$	$\mathrm{Nu}_a = \mathrm{Sh}_a = 0.66599\mathrm{Ra}^{0.2002}N^{0.4114}$

$-10 \leq N \leq 10$. Figure 13 shows the comparison between numerical results and the correlations in Table 3.

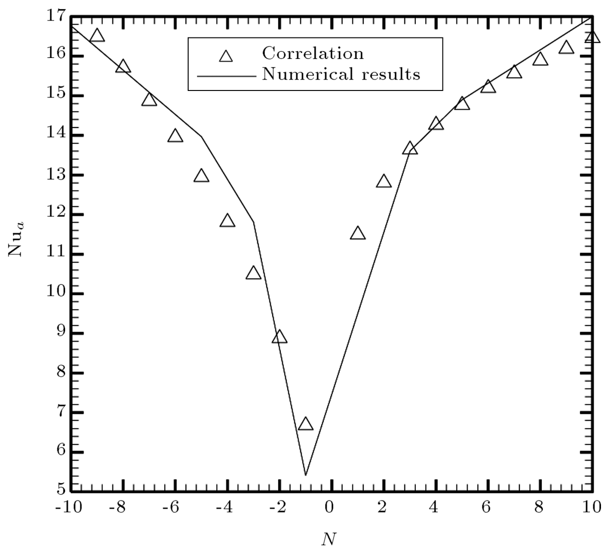

Figure 13. Comparison between numerical results and the correlation for Ra = 10^5 and Le = 1.

5. Conclusion

In this article, simultaneous natural convection heat and mass transfer around a hot body in a rectangular air-filled cavity was studied numerically. According to the present numerical results, the following conclusions are drawn:

1. By increasing the absolute value of Buoyancy ratio, the average Nusselt and Sherwood numbers increase.
2. By incresing Lewis number, the average Sherwood number increases but the average Nusselt number decreases.
3. By increasing Rayleigh number, the average Nusselt and Sherwood numbers increase at Le=1 and $N = 1$.
4. The predicted values of average Sherwood and Nusselt numbers in the range investigated for buoyancy ratio, Rayleigh and Lewis numbers are correlated.

Nomenclature

C Concentration
C Dimensionless concentration

CCW	Counterclockwise
CW	Clockwise
D	Mass diffusivity
H	Enclosure height
L	Enclosure length
Le	Lewis number (Sc/Pr)
N	Buoyancy ratio
Nu	Nusselt number
p	Pressure
P	Dimensionless pressure
Pr	Prandtl number
Ra_M	Mass transfer Rayleigh number
Ra_T	Heat transfer Rayleigh number
Sc	Schmidt number
Sh	Sherwood number
T	Temperature
u, v	Components of velocity
U, V	Dimensionless velocity components
W	Body length
x, y	Cartesian coordinates
X, Y	Dimensionless Cartesian coordinates

Greek symbols

α	Thermal diffusivity
Ψ	Streamfunction
θ	Dimensionless temperature
v	Kinematic viscosity
β_T	Volumetric coefficient of thermal expansion
β_M	Volumetric coefficient of expansion with concentration

Subscript

a	Average
c	Cold wall
h	Hot wall
T	Thermal
M	Mass

References

1. Davis, D.V. "Natural convection of air in a square cavity: A benchmark numerical solution", *Int. J. Numer. Methods Fluid*, **3**, pp. 249-264 (1983).
2. Ostrach, A. "Natural convection in enclosures", *J. Heat Transfer*, **110**, pp. 1175- 1190 (1988).
3. Lin, D.S. and Nansteel, M.W. "Natural convection heat transfer in a square enclosure containing water near its density maximum", *Int. J. Heat Mass Transfer*, **30**, pp. 2319-2329 (1987).
4. Nansteel, M.W., Medjani, K. and Lin, D.S. "Natural convection of water near its density maximum in rectangular enclosure: low Rayleigh number calculations", *Phys. Fluids*, **30**, pp. 312-317 (1987).
5. Tong, W. and Koster, J.N. "Coupling of natural convection flow across a vertical density inversion interface", *Warme. Stoffubertrag*, pp. 471-479 (1993).
6. Tong, W. "Aspect ratio effect on natural convection in water near its density maximum temperature", *Int. J. Heat Fluid Flow*, **20**, pp. 624-633 (1999).
7. Ho, C.J. and Tu, F.J. "Transition to oscillatory natural convection of water near its density maximum in a tall enclosure", *Int. J. Num. Methods Heat Fluid Flow*, **11**, pp. 626-641 (2001).
8. Hossain, M.A. and Rees, D.A.S. "Natural convection flow of water near its density maximum in a rectangular enclosure having isothermal walls with heat generation", *Heat Mass Transfer*, **41**, pp. 367-374 (2005).
9. Kandaswamy, P., Sivasankaran, S. and Nithyadevi, N. "Buoyancy-driven convection of water near its density maximum with partially active vertical walls", *Int. J. Heat Mass Transfer*, **50**, pp. 942-948 (2007).
10. Nithyadevi, N., Sivasankaran, S. and Kandaswamy, P. "Buoyancy-driven convection of water near its density maximum with time periodic partially active vertical walls", *Meccanica*, **42**, pp. 503-510 (2007).
11. Lee, J.R. and Ha, M.Y. "A numerical study of natural convection in a horizontal enclosure with a conducting body", *Int. J. Heat and Mass Transfer*, **48**, pp. 3308-3318 (2005).
12. Das, M. and Reddy, K. "Conjugate natural convection heat transfer in an inclined square cavity containing a conducting block", *Int. J. Heat and Mass Transfer*, **49**, pp. 4987-5000 (2006).
13. Sheikhzadeh, G., Fattahi, A. and Mehrabian, M. "Numerical study of steady magneto convection around an adiabatic body inside a square enclosure in low Prandtl numbers", *Heat Mass Transfer*, **47**, pp. 27-34 (2011).
14. Sheikhzadeh, G., Fattahi, A., Mehrabian, M. and Pirmohammadi, M. "Effect of geometry on magneto-convection in a square enclosure filled with a low Prandtl number fluid", *Journal of Process Mechanical Engineering*, pp. 53-61 (2011).
15. Gebhart, B. and Pera, L. "The nature of vertical natural convection flows resulting from the combined buoyancy effects of thermal and mass diffusion", *Int. J. Heat and Mass Transfer*, **14**, pp. 2025-2050 (1971).
16. Bejan, A. "Mass and heat transfer by natural convection in a cavity", *Int. J. Heat and Fluid Flow*, **6**(3), pp. 149-159 (1985).

17. Wee, H.K., Keey, R.B. and CunnIingham, M.J. "Heat and moisture transfer by natural convection in a rectangular cavity", *Int. J. Heat and Mass Transfer*, **32**(9), pp. 1765-1778 (1989).

18. Nishimura, T., Wakamatsu, M. and Morega, A.M. "Oscillatory double-diffusive convection in a rectangular enclosure with combined horizontal temperature and concentration gradients", *Int. J. Heat Mass Transfer*, **41**, pp. 1601-1611 (1998).

19. Ben Snoussi, L., Chouikh, R. and Guizani, A. "Numerical study of the natural convection flow resulting from the combined buoyancy effects of thermal and mass diffusion in a cavity with differentially heated side walls", *Desalination*, **182**, pp. 143-150 (2005).

20. Chouikh, R., Ben Snoussi, L. and Guizani, A. "Numerical study of the heat and mass transfer in inclined glazing cavity: application to a solar distillation cell", *Renew Energy*, **32**, pp. 1511-1524 (2007).

21. Nithyadevi, N. and Yang, R-J. "Double diffusive natural convection in a partially heated enclosure with Soret and Dufour effects", *International Journal of Heat and Fluid Flow*, **30**(5), pp. 902-910 (2009).

22. Nikbakhti, R., Rahimi, A.B. "Double-diffusive natural convection in a rectangular cavity with partially thermally active side walls", *J. Taiwan Inst. Chem. Eng.*, **43**, pp. 535-541 (2012).

23. Al-Amiri, A., Khanafer, K. and Pop, I. "Numerical simulation of combined thermal and mass transport in a square lid-driven cavity", *Int. J. Thermal Science*, **46**, pp. 662-671 (2007).

24. Teamah, M. and Maghlany, W. "Numerical simulation of double-diffusive mixed convective flow in rectangular enclosure with insulated moving lid", *Int. J. Thermal Science*, **49**, pp. 1625-1638 (2010).

25. Ray Mahapatra, T., Pal, D. and Mondal, S. "Effects of buoyancy ratio on double-diffusive natural convection in a lid-driven cavity", *International Journal of Heat and Mass Transfer*, **57**(2), pp. 771-785 (2013).

Biographies

Ghanbar Ali Sheikhzadeh is an Associate Professor of Mechanical Engineering Department at University of Kashan, Kashan, Iran. He received his PhD in Mechanical Engineering from Shahid Bahonar University of Kerman. His research works concern numerical analysis and application of heat transfer in nano-systems and other areas of thermal and fluid sciences. Dr. Sheikhzadeh has published many papers in journals and conferences in his research fields.

Roghayeh Heydari received her MS degree in Mechanical Engineering at University of Kashan, Kashan, Iran. Her research interests focus on numerical analysis of heat and mass transfer in nano-systems and other areas of thermal and fluid applications. Her research works are also paid to combustion systems such as numerical investigations of flames and furnaces.

Najmeh Hajialigol is a PhD student at Tarbiat Modares University of Tehran, Tehran, Iran. She received her MSc degree from University of Kashan, Kashan, Iran. Her research activities are paid to combustion, computational fluid dynamics and heat transfer.

Abolfazl Fattahi is a PhD student at Iran University of Science and Technology, Tehran, Iran. He received his MSc degree from University of Kashan, Kashan, Iran. His research activities are paid to combustion, numerically and empirically, computational fluid dynamics and heat transfer.

Mosaffar Ali Mehrabian is a full professor at Shahid Bahonar University of Kerman, Kerman, Iran. He received his PhD degree from University of Bristol, England. His researches are focused on fluid mechanics, thermodynamics and heat transfer.